Physicochem. Probl. Miner. Process., 58(3), 2022, 145667

http://www.journalssystem.com/ppmp

Physicochemical Problems of Mineral Processing

ISSN 1643-1049

Selective comminution and grinding mechanisms of spent carbon anode from aluminum electrolysis using ball and rod mills

Chao Ni [1], Shaoqi Zhou [1], Jixuan Gao [1], Xiangning Bu [1], Yuran Chen [2], Muidh Alheshibri [3, 4], Guangyuan Xie [1], Biao Li [5],

[1] Key Laboratory of Coal Processing and Efficient Utilization (Ministry of Education), School of Chemical Engineering and Technology, China University of Mining and Technology, Xuzhou 221116, China

[2] School of Materials Science and Engineering, Zhengzhou University, Zhengzhou 450001, Henan, China

[3] Department of Basic Sciences, Deanship of Preparatory Year and Supporting Studies, Imam Abdulrahman Bin Faisal University, P.O. Box 1982, Dammam 31441, Saudi Arabia

[4] Basic & Applied Scientific Research Center, Imam Abdulrahman Bin Faisal University, P.O. Box 1982, Dammam 31441, Saudi Arabia.

[5] Minerals Research Laboratory, College of Engineering, North Carolina State University, Asheville, NC, 28801, USA

Corresponding authors: xiangning.bu@foxmail.com, xiangning.bu@cumt.edu.cn (X. Bu); cyr_hy@zzu.edu.cn (Y. Chen)

Abstract: The recovery of spent carbon anode (SCA) materials plays important roles in environment protection and resources recycling, while this cannot be efficiently achieved without liberation. In this study, grinding characteristics of spent carbon anode from aluminum electrolysis in both ball mill and rod mill were analyzed, and compared based on the utilization of the selective Fuerstenau upgrading curves. In addition, the different grinding mechanisms of ball and rod milling were evaluated by analyzing the shape factor and surface roughness of the ground samples. Results of mineralogical characterizations indicated that carbon particles (d_{50} = 46.86 μm) presented in the SCA were closely associated with cryolite particles. At 5 min grinding time, the maximum selective comminution factor (β) values of ball milling and rod milling were 2.00 and 1.63, respectively, indicating a higher degree of selective comminution of SCA was achieved from ball milling. Comparisons of the valuable component content (c_v, cum) of -125 μm ground particles and the shape characterizations of 74–125 μm ground particles generated from ball and rod milling manifest that a direct relationship exists between the degree of selective comminution and the grinding mechanism.

Keywords: selective comminution, ball mill, rod mill, spent carbon anode, grinding mechanism

1. Introduction

The International Aluminum Institute (Institute, 2020) reported that the global production of primary aluminum tapped from electrolytic cells (or pots) during the electrolytic reduction of metallurgical alumina (aluminum oxide) was 63,697 thousand metric tons (t) in 2019. Further, China is the largest producer of aluminum (35,795 thousand t in 2019), accounting for 56.20% of global production. Spent carbon cathode (SCC) is the carbon cathode of the Hall–Héroult cell, eroded by high-temperature molten salt and metallic sodium (Grjotheim et al., 1982). Approximately 24–30 kg of SCC is generated from 1 t of aluminum production (Holywell and Breault, 2013). In addition, the carbon anode of aluminum reduction cell is damaged and dropped in the reduction cell due to the selective oxidation of anode, erosion of electrolytes, secondary reaction in reduction process and mechanical damage during operation (Grjotheim et al., 1982; Li et al., 2015). This process results in the presence of the floating carbon residues on the surface of the aluminum reduction cell, which is separated by artificial fishing (Xu et al., 2009). Approximately 5-15 kg spent carbon anode (SCA) is continuously generated from 1 t of aluminum production (Chen et al., 2009). Thus, it has been estimated that the world's aluminum smelters generated 1,528–1,910 thousand t of SCC and 318–955 thousand t of SCA in 2019. It is commonplace for SCC and SCA to be disposed of in landfills, posing a risk of soil contamination due to

DOI: 10.37190/ppmp/145667

the leaching of soluble fluoride and highly toxic cyanide (Sleap et al., 2015). SCC and SCA have been listed in the national list of hazardous wastes by China in 2016 (Yang et al., 2020b). Moreover, SCC and SCA also contain carbon, fluoride, alumina, cryolite, aluminosilicate, and a trace of cyanide, which is a recoverable resource (Flores et al., 2017). Accordingly, from the perspective of resource recycling and environmental protection, it is important to achieve effective green treatment and highly efficient recoveries of SCC and SCA.

The importance of comprehensive use of solid waste (SCC and SCA) in aluminum smelters is in the recovery of valuable materials (carbon and cryolite) and the harmless treatment of fluoride and cyanide. There are two major categories of SCC treatment methods: pyrometallurgical and hydrometallurgical (Bishoyi, 2015; Tropenauer et al., 2019). Pyrometallurgical processes is used for the industrial recycling of solid waste because they facilitate the harmless treatment of solid waste to remove toxic fluoride and cyanide (Bruno, 2003; Chai et al., 2016; Personnet, 2013; Xie et al., 2020; Zhou, 2015; Zou et al., 2018). However, valuable components such as carbon and cryolite are usually lost in slag during the process (Flores et al., 2017; Shi et al., 2012; Yang et al., 2020a; Zou et al., 2018). Moreover, high energy consumption, high equipment investment, and environmental pollution also hinder the wide application of pyrometallurgical processes. Consequently, various hydrometallurgical processes have been developed to treat and recycle SCC and SCA, including flotation and chemical leaching (Tropenauer et al., 2019; Yang et al., 2020b).

Flotation is an effective method of selectively separating hydrophobic carbon from hydrophilic cryolite following the comminution and grinding processes of SCC and SCA. As shown in Table 1, a concentrate with 96.10% carbon content and tailings with 4.10% carbon content can be obtained using a four-stage flotation circuit; however, further upgrading by flotation is challenging. SinghMaitra (1986) introduced a method for recovering carbon and fluoride (while also reducing pollution) by recycling flotation tailings of aluminum smelters. Tropenauer et al. (2019) developed a technique for combing flotation and carrying out chemical treatment to produce purified carbon and silicate fractions from industrial waste (primary aluminum production). It is worth noting that while chemical leaching (acid, soluble aluminum salt solution, and caustic) is more effective than flotation techniques for purifying SCC and SCA (Xiao et al., 2018; Yang et al., 2020b), it can cause severe environmental problems.

Table 1. Summary of flotation studies of SCC and SCA

Solid waste	Carbon content of raw ore (%)	Grinding Method	Number of flotation stages	Carbon content (%)		Ref.
				Concentrate	Tailings	
SCC	71.20	Ball mill	4	96.10	4.10	(Li et al., 2013)
	49.10			85.30	19.80	(Li et al., 2013)
	36.10			73.10	26.60	(Li et al., 2013)
	51.33	Ball mill	3	91.20	5.50	(Lu and Qiu, 1997)
SCA	30.50	Rod mill	3	94.59	1.01	(Mei et al., 2016)

Prior to flotation, SCC and SCA are commonly comminuted and ground to disassociate carbon from cryolite (see Table 1). While grinding-flotation circuits have been widely used for SCC and SCA treatment, differences in selective comminution between ball and rod mills have not yet been analyzed systematically. Selective comminution is a promising method for reducing specific energy consumption. Moreover, appropriate selective comminution preconcentrates the ore and removes the coarse liberated gangue before entering the subsequent milling circuit, which is a potential strategy for substantial energy saving (Hesse et al., 2017; Lowes et al., 2018). Selective comminution is the result of a comminution system that comprises appropriate comminution parameters (such as operational parameters and the design of the comminution machine) and inherently suitable material properties (Hesse, 2014; Stepanov et al., 1991). The different distributions of valuable and waste minerals (as a function of particle size) are commonly employed to characterize selective comminution qualitatively (Hesse et al., 2017). Hesse et al. (2017) defined the parameters to quantify selectivity (S) and η_{ore}, where SZ quantified the change in selectivity between the feed material and product. They confirmed that selective comminution requires a systemic approach—comminution behavior of the ore under a certain load, type of comminution machine, and number of operational parameters of the system. A Fuerstenau upgrading diagram with recovery plots is another method for estimating selective comminution, which has been used to study the selective comminution of quartz-topaz glimmer Greisen ore(Leißner et al., 2014), iron ore(Reichert et al., 2015), and spent lithium-ion batteries(Widijatmoko et al., 2020).

Some researchers have paid attention to the differences in the grinding mechanisms of ball and rod mills, which commonly results in the following variations: the shape properties of ground particles (Hicyilmaz et al., 2004; Ulusoy, 2008b; Ulusoy and Kursun, 2011), the residence time distribution (RTD) of particles(Gupta and Patel, 2015), the size distribution of ground products (Foszcz et al., 2018), and the flow characteristics of the tracer particles (dolomite, magnetite, and galena)(Abouzeid and Fuerstenau, 2012). AbouzeidFuerstenau (2012) reported that rod mill products have a narrow size distribution compared to those from a ball mill, which is partly attributable to the plug flow mode of the material transport in the rod mill and partly to the well-known bridging action of the rods. Foszcz et al. (2018) found that ball mills are more efficient in terms of incrementally small-sized fractions compared to rod mills. Moreover, based on probability theory, Malyshev et al. (2017) revealed that rod mills have superior capacity for comminuting large particles compared to ball mills due to the combined effect of steric and activation factors. FoszczGawenda (2012) demonstrated that ball mills were optimum for fine grinding (<0.1 mm) while rod mills were efficient for thicker and harder particles in the feed. It is believed that the line load on particles in rod mills helps to break hard materials (Gupta and Yan, 2016). By comparison, the point load on the particles in ball mills is conducive to the attrition process (Bu et al., 2019b; Bu et al., 2020a). Abrasion and attrition result in rounder (more spherical) ball-milled particles with smoother surfaces than rod-milled particles (Bu et al., 2019a; Hicyilmaz et al., 2004; Ulusoy, 2008b; Ulusoy and Kursun, 2011). However, it is found that there is no related study on the difference of selective comminution of SCA between ball and rod mills.

Accordingly, the objective of this study was to compare the selective comminution of SCA using ball and rod mills. The degree of selective comminution was estimated based on Fuerstenau upgrading curves. In particular, the different degrees of selective comminution were associated with the different breakage mechanisms of ball and rod milling. In addition, it is notable that the comparison between ball and rod milling is only a preliminary study because of the lack of the optimization of the operating conditions for ball and rod milling, such as wet and dry grinding, rotational speed of grinding devices, and the filling fractions of grinding medium and powder samples. The effects of those factors on the selective comminution of spent carbon anode from aluminum electrolysis will be presented in the future research.

2. Materials and methods

2.1. Sample preparation

A spent carbon anode (SCA) sample was obtained from an aluminum and power company (Shandong Weiqiao Aluminum & Electricity Co., Ltd., Binzhou, Shandong Province, China) in the form of −1 mm powder. The SCA sample was mixed by thorough coning and quartering, and representative sub-samples were obtained for sieving, X-ray diffraction (XRD), X-ray fluorescence (XRF), and grinding tests.

2.2. Sieving test

The sample was sieved using a set of 1000, 500, 250, 125, 74, and 45 μm sieves (ASTM E11). The industry standard YS/T 273.2-2006 (for the chemical analysis and physical properties of cryolite, part 2: determination of ignition loss) was used to evaluate the approximate loss on ignition (LOI, %). This value of LOI was then used to represent the approximate carbon content of the products obtained from the sieve analysis.

2.3. Grinding test

The grinding tests were carried out in dry conditions. Ball milling tests were performed using a QM-5 laboratory-scale ball mill (Changsha Tianchuang Powder Technology Co., Ltd., Changsha, China). The diameter and the length of the drum for the ball mill were 12.5 and 16.0 cm, respectively. A 2.0 L stainless steel cylinder was used as the drum in the ball milling tests, in which 2.22 kg of stainless steel balls with diameters of 1.20, 0.90, 0.62, and 0.55 cm were used. The weight percentages of the stainless steel balls were 33.75%, 31.40%, 18.37%, and 16.48%, respectively. The operational speed was 115 rpm, and a 200 g mass of −1 mm feed sample material was used for the ball milling tests.

The critical rotational speed for centrifuging in ball and rod milling can be calculated as follows (Abouzeid and Fuerstenau, 2012):

$$N_c = \frac{30}{\pi}\sqrt{\frac{2g}{D-d_r}} \tag{1}$$

where d_r is the diameter of the rod. For this study, the critical rotational speed for the rod mill was 138–140 rpm (dependent on rod diameter) with a feed size of –1 mm and operating speed of 50 rpm, respectively.

Compared to the commonly used Eq. 1, the following Eq., related to a variety of parameters (including the ball diameter d, the volume fill fraction φ of material within the tumbler, and the material angle β_s of repose), was applied to calculate the critical rotational speed for ball milling (Bu et al., 2019b; Juarez et al., 2011; Kallon et al., 2011; Walton and Braun, 1993):

$$N_c = \frac{30}{\pi}\sqrt{\frac{2g}{(D-d_b)\sin\beta_s\sqrt{1-\varphi}}} \tag{2}$$

here, D and d_b are the diameters of the drum and ball, respectively. The critical rotational speed for the ball mill was 183–188 rpm, with the variation caused by different ball diameters.

Rod milling tests were conducted using a KJXMB III laboratory-scale rod mill (Yancheng Kejie Test Instrument Factory, Yancheng, Jiangsu Province, China) equipped with a 1.2 L stainless steel cylinder (D x L: 10.5 cm x 14.0 cm). The grinding tests were carried out using rods of 1.1, 1.3, and 1.5 cm diameters and the weight percentages of the stainless steel rods (length = 14 cm) were 30.37%, 34.96%, and 34.67%, respectively. During the rod milling tests, the operational speed of the rod mill, the weight of the stainless steel rods, and the weight of the feed sample (−1 mm) were 50 rpm, 3.16 kg, and 200 g, respectively.

2.4. XRD and XRF tests

The sample was ground to a fine powder (<200 mesh size) using an XPM-ϕ 120 × 3 three-headed grinding machine (Nanchang Source of Mining and Metallurgy Equipment Co., Ltd., Nanchang, China). The XRD and XRF analyses were performed using a D8 Advance X-ray diffractometer (Bruker, Germany) and an S8 TIGER X-ray fluorescence spectrometer (Bruker, Germany), respectively. The detailed operating procedure for the XRD measurements has already been described in the literature (Bu et al., 2017; Chang et al., 2020).

2.5. Polarized light microscopy measurement

Thin sections of the SCA sample were prepared by Beijing Riyueshi Mining Technology Development Co., Ltd. (Beijing, China), and photographs of them were taken using a CX40P-series polarizing microscope (Sunny Optical Technology Co. Ltd).

2.6. Shape factor measurement

A 3D dynamic image analysis (Micromeritics® Instrument Corp., Norcross, USA) was conducted to characterize the circularity of the ground products produced by the ball and rod mills. Detailed working procedures and measurement principles for this apparatus can be found in the literature (Ulusoy and Igathinathane, 2014). Circularity (C) is computed from the projected area and bounding circle diameter, which is a dimensionless ratio. Round particles is valid for C=1 and elongated particles is valid for C<1 especially when C approaches to zero. Accordingly, this can be considered a fraction of the bounding circle's area covered by the actual projected area of the particle (Ulusoy and Igathinathane, 2014).

2.7. Surface roughness measurement

Scanning electron microscopy (SEM) analysis was carried out using an FEI Quanta 250 SEM system (FEI Company, Hillsboro, Oregon, USA). Detailed information on the SEM analysis can be found in the literature (Bu et al., 2017). The SEM measurement results can only offer a qualitative comparison of roughness of ground particles produced by ball and rod milling. It is notable that the perimeter and area of the particles by 2 D can be calculated based on the axis measurement of the SEM images (Ulusoy et al., 2003; Ulusoy, 2008a). In addition, BET (Brunauer, Emmett and Teller) gas adsorption techniques can be used to calculate a surface roughness factor (Hicyilmaz et al., 2005; Hicyilmaz et al., 2006; Yekeler and Ulusoy, 2004). In this study, the surface roughness was also calculated quantitatively based on the BET results from the following relationship given in Eq. (3) (Gungoren et al., 2019; Guven et al., 2015):

$$\Lambda = \frac{\rho \cdot d_{AVG} \cdot A_{BET}}{6} \tag{3}$$

here, ρ is the density of the solid, d_{AVG} is the mean size of the size fraction, and A_{BET} is the specific surface area calculated using the BET isotherm. In this study, the specific surface areas (area per unit mass or volume) of the ground products obtained from ball and rod milling were determined using a Quantachrome™ Autosorp-1 MP device with N_2 gas using optimized protocols.

3. Results and discussion

3.1. Characterization of SCA

The LOI of the SCA sample was 12.29%. However, according to China Standard GB/T 4291-2017 (for synthetic cryolite), the LOI of the cryolite product should be <2.5%. This means the SCA sample contained approximately 10% carbon, which originated from the carbon anode during aluminum electrolysis. Purified carbon can be used to synthesize silicon carbide (SiC) (Yuan et al., 2018), be recycled as a low-cost material for the anodes of Li-ion batteries(Yang et al., 2020a), and present an accepted energy potential for various ironmaking applications(Flores et al., 2017). The chemical composition of the raw sample is given in Table 2. The SCA sample contained more in fluorine (F, 53.90%), sodium (Na, 26.70%), and aluminum (Al, 16.56%), although it was lacking in calcium (Ca, 2.67%). The XRD patterns of the SCA sample are shown in Fig. 1. The mineral components of the SCA sample were cryolite and corundum, which accorded well with the content of major elements obtained from the XRF analysis shown in Table 2. Cryolite, rather than corundum, was considered the main mineral.

Table 2. Major element constituents from the XRF analysis

Element	F	Na	Mg	Al	Si	S	K	Ca
Wt. (%)	53.90	26.70	0.28	16.56	0.11	0.38	0.19	2.67

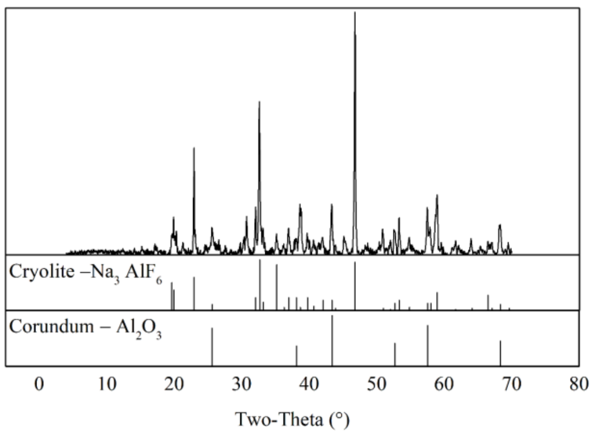

Fig. 1. XRD patterns of the SCA sample with respect to mineral identification

Fig. 2 presents the size distribution of the SCA sample. The LOI value was used to represent the approximate content (c_w) of the waste component. The content (c_v) of the valuable component was calculated as $c_v = 100 - \mathrm{LOI}$. As shown in Fig. 2, c_v increased significantly from 9.17% to 64.13% with increasing particle size (from <45 μm to 500–1,000 μm), indicating that most of carbon material consisted of larger sized fractions. Observations of thin sections of the SCA sample are presented in Fig. 3. Fig. 3

(a) and (b) indicate that there were many carbon particles >100 μm in a state of dissociation. Fig. 3(d) indicates that large cryolite particles were associated with carbon materials. These phenomena resulted in a high waste component content with size classes coarser than 0.5 mm (see Fig. 2 (b)). It can also be observed from Fig. 3 that a larger number of locked particles (marked by blue squares) existed in the SCA sample where the carbon material was strongly embedded in cryolite particles. Fig. 4 presents the size distribution of carbon particles in the SCA sample. The sizes of carbon particles of microscope photos were estimated using ImageJ software. The calculation method of the cumulative size distribution of carbon particles referred to the literature (Bu et al., 2020a; Dunbar and Hickey, 2000). It was observed that the size distribution of the carbon particles in the SCA sample had an average size (d_{50}) of 46.86 μm, while the d_{50} of the SCA sample was approximately 125 μm. Therefore, it was necessary to liberate the valuable component from the waste component by efficient breakage.

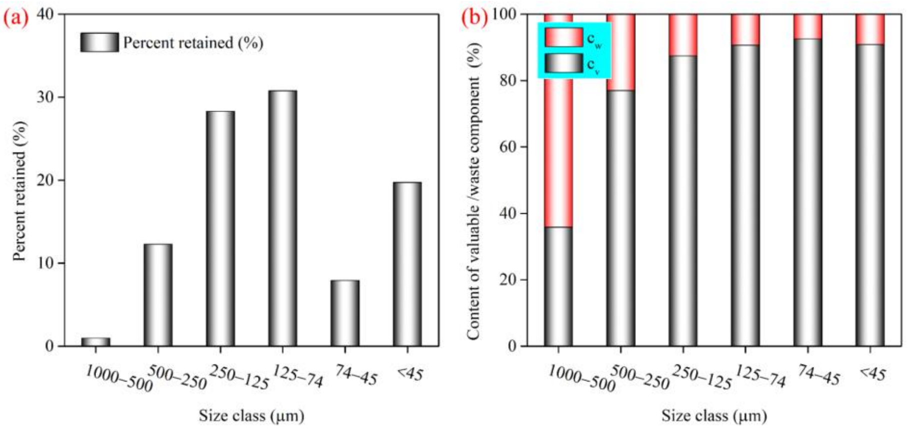

Fig. 2. Size distribution of the SCA sample: (a)-% retained; (b)-content of valuable/waste component

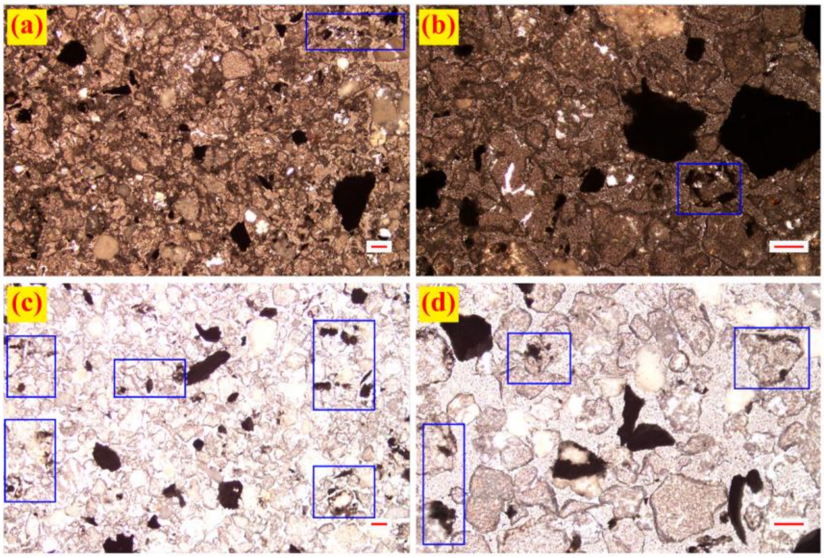

Fig. 3. Microscope photographs of thin sections of the SCA sample. Images (a) and (b) were taken from thin sections of the raw ore, while (c) and (d) were taken from thin sections of a + 45 μm size fraction. The length of the red line represents 100 μm

3.2. Comparison of selective comminution using ball and rod mills

For a given t_d (a certain separation cut size), the ground product could be separated into two fractions: fine and coarse. Moreover, the calculated recoveries of valuable (R_v) and gangue (R_w) materials for various t_d values could be plotted diagrammatically. The calculated recovery of valuable, R_v, material is the cumulative recovery of this component with size classes finer than the selected sieve size (undersized product):

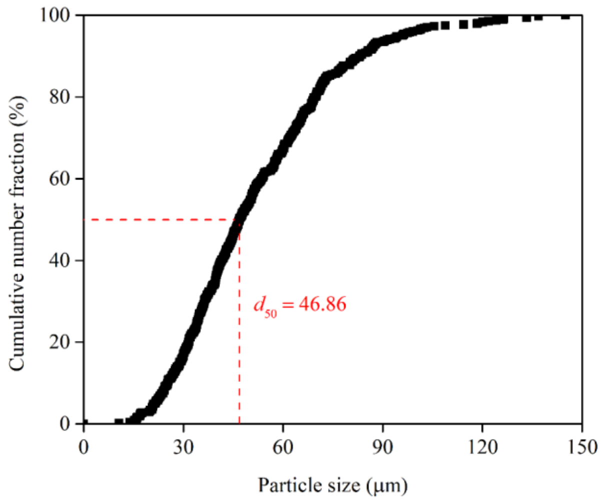

Fig. 4. Size distribution of carbon particles in the SCA sample.

$$R_V = \frac{\sum_{i=1}^{N} \omega_{V,i} \cdot c_{V,i}}{\sum_{i=1}^{M} \omega_{V,i} \cdot c_{V,i}} \tag{4}$$

here, N is the number of the size class smaller than the selected sieve size, M is the total number of the size class obtained from sieving analysis, $w_{V,i}$ is the weight percentage (valuable material) of the size class i, and $c_{V,i}$ is the content of the valuable material in size class i.

The calculated recovery of gangue, R_w, material is :

$$R_W = \frac{\sum_{i=1}^{N} \omega_{W,i} \cdot c_{W,i}}{\sum_{i=1}^{M} \omega_{W,i} \cdot c_{W,i}} \tag{5}$$

here, N is the number of the size class smaller than the selected sieve size, M is the total number of the size class obtained from sieving analysis, $w_{W,i}$ is the weight percentage (gangue material) of the size class i, and $c_{W,i}$ is the content of the component (gangue material) in size class i.

The recovery plots for ball and rod milling are presented in Fig. 5 (applied to the coarse fraction). Drzymala and Ahmed (2005) used various mathematical formulae (including formulas with one, two, or more adjustable parameters) to approximate the separation results in a Fuerstenau upgrading graph. According to the plot shape shown in Fig. 5, the two exponential asymmetric Eqs. were modified to approximate the effectiveness of selective comminution for the recovery plots (applied to the coarse fraction) as follows:

$$R_{cum,V} = \frac{100^{\alpha} - \left(100 - R_{cum,W}\right)^{\alpha}}{100^{\alpha-1}} \tag{6}$$

$$R_{cum,V} = \frac{{R_{cum,W}}^{\beta}}{100^{\beta-1}} \tag{7}$$

here, α and β are adjustable parameters for Eqs. 6 and 7, respectively, and they are the selective comminution factors. When α (or β) = 1 (dashed line in Fig. 5), there was no selective comminution between the valuable and waste components. When $\alpha > 1$ (or $0 < \beta < 1$), selective comminution existed for the coarse fraction. Finally, when $0 < \alpha < 1$ (or $\beta > 1$), selective comminution existed for the fine fraction.

Comparisons of the fitting performance of Eqs. 6 and 7 using *RMSE* (root mean square error) and Adj. R^2 are displayed Table 3. The parameters of Eqs. 6 and 7 were evaluated via the nonlinear least squares function of MATLAB software. A smaller *RMSE* (or a greater Adj. R^2) indicates a better fitting performance of a model. It is observed that most of *RMSE* values were smaller than 3 and most of Adj. R^2 were greater than 0.97. The magnitudes of *RMSE* and Adj. R^2 were consistent with the literature (Bu et al., 2016; Bu et al., 2020b; Yang et al., 2021). Both Eqs. 6 and 7 provided an acceptable fitting performance from the viewpoint of statistical analysis. However, the *RMSE* for the fitted data using Eq. 6 was relatively less than that using Eq. 7 for both ball and rod milling. Moreover, the adj. R^2 obtained with Eq. 7 was relatively greater than for Eq. 6, and a comparison of the Fuerstenau upgrading curves was fitted by Eqs. 6 and 7 at a grinding time of 5 min. Furthermore, comparisons of the Fuerstenau upgrading curves fitted by Eqs. 6 and 7 (Fig. 6) indicated that Eq. 7 had a superior ability to describe Fuerstenau upgrading curve compared to Eq. 6. Thus, it is concluded that the assessment results indicated that Eq. 7 exhibited superior fitting performance compared to Eq. 6.

Table 3. Comparisons of the fitting performance (*RMSE* and Adj. R^2) of Eqs. 6 and 7

Grinding time (min)	Ball milling				Rod milling			
	Eq. 6		Eq. 7		Eq. 6		Eq. 7	
	RMSE	Adj. R^2	*RMSE*	Adj. R^2	*RMSE*	Adj. R^2	*RMSE*	Adj. R^2
0	5.83	0.9798	1.68	0.9983	5.83	0.9798	1.68	0.9983
5	7.1	0.9688	1.83	0.9979	5.33	0.9831	1.29	0.999
10	7.4	0.9683	3.47	0.9992	5.53	0.9815	1.47	0.9987
20	3.98	0.9882	1.49	0.9983	5.22	0.9825	2.95	0.9944
30	3.8	0.9893	1.75	0.9977	5.38	0.981	3.3	0.9929
60	1.28	0.999	0.33	0.9999	5.31	0.9842	3.62	0.9926

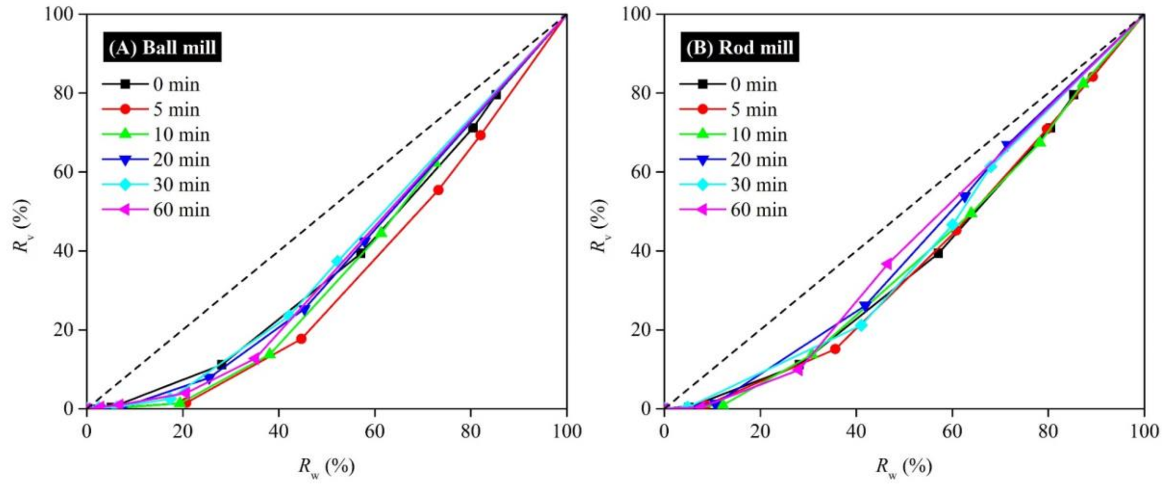

Fig. 5. Recovery plots for the Fuerstenau upgrading curves for ball and rod milling (applied to the coarse fraction). The original data including the separation cut size were attached in the appendix

Eq. 6 was used to calculate the selective comminution factor (β) for ball and rod milling. Fig. 7 presents a comparison of the calculated β for ball and rod milling at various grinding times. The β values for the ball milling at various grinding times were greater than those of the feed material (β = 1.6). By comparison, the β value for the rod milling was less than that for the feed material when the grinding time was >10.47 min (approximately). At 5 min grinding time, the ball and rod milling had maximum β values of 2.00 and 1.63, respectively. These results indicated that ball milling performed more effectively than rod milling for selective comminution.

3.3. Relationship between grinding mechanisms and selective comminution

The valuable component content ($c_{v,\,cum}$) of –125 µm ground particles produced for various ball and rod milling times are presented in Fig. 8. Cryolite (2.5–3) has a similar level of Mohs hardness to gypsum (Mohs hardness: ~2.2) (Pauly, 1985); thus, the compression strength of cryolite is approximated to that of gypsum, which ranges from 1.5 to 6.7 MPa. According to the difference in Mohs hardness, the cryolite and carbon present in the SCA were considered the weaker material and the stronger mineral, respectively. Moreover, the XRF and XRD analyses indicated that cryolite was the major mineral for this SCA. In this study, the magnitude of $c_{v,\,cum}$ approximately equalled the cryolite content. When the grinding time was < 10 min, the $c_{v,\,cum}$ of the –125 µm ground particles from rod milling were smaller than from ball milling. This revealed that rod milling had superior breakage ability for stronger minerals (carbon) compared to ball milling. Gupta and Yan (2016) concluded that the line load was more conducive to the breakage of hard materials than the point load on the particles produced by ball mills,

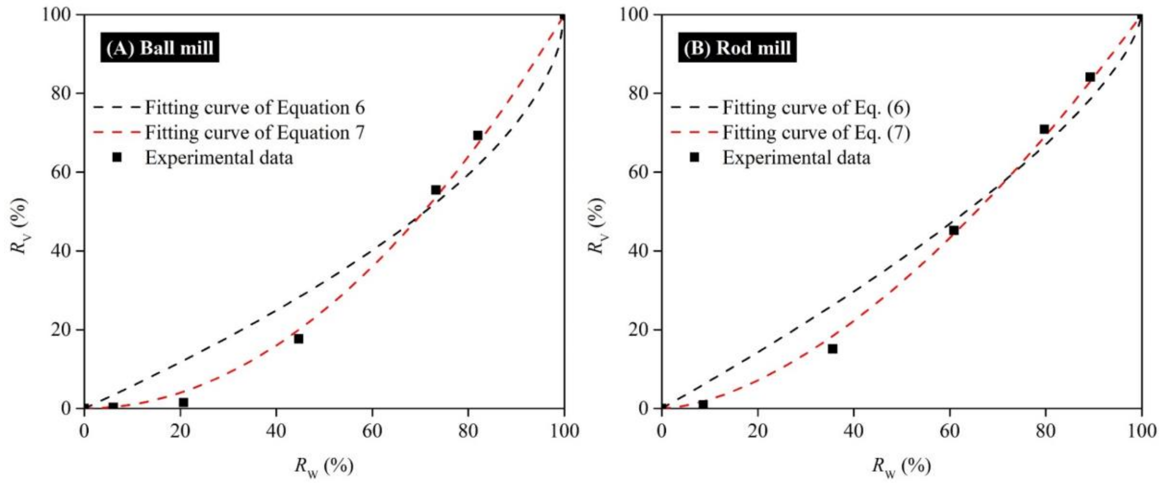

Fig. 6. Comparisons of the Fuerstenau upgrading curves fitted by Eqs. 6 and 7: (A) ball milling; (B) rod milling. The experimental data were the recovery plots for ball and rod milling at 5 min grinding time

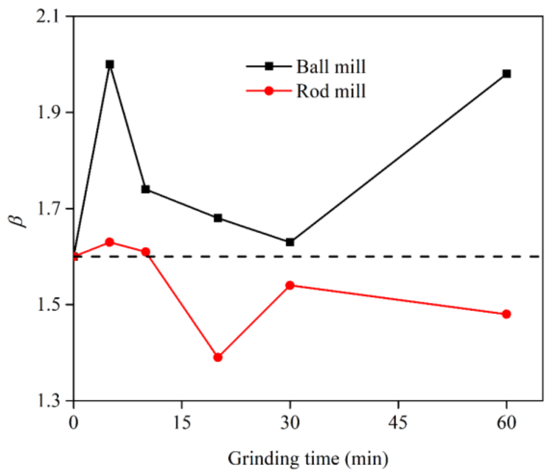

Fig. 7. Comparison of the selective comminution factor β for ball and rod milling at various grinding times

which was consistent with the findings of this study. When the grinding time was >10 min, the $c_{v,\,cum}$ of the –125 µm ground particles for both ball and rod milling decreased constantly as the grinding time further increased. With this increased grinding time, increasing numbers of carbon and cryolite particles were fractured into smaller particles, which increased the difficulty of selective separation and the consumption of grinding energy. Compared to the raw sample (0 min grinding time, $c_{v,\,cum}$ = 90.98%), the $c_{v,\,cum}$ of the –125 µm ground particles produced by ball milling increased and reached a peak of 91.39 % at a grinding time of 5 min, which was consistent with the estimated results for the selective comminution for ball milling (see Section 3.2). Meanwhile, the –125 µm ground product of the rod mill had a smaller $c_{v,\,cum}$ than the raw sample, indicating that the stronger mineral was fractured by rod milling in larger quantities. This resulted in a deterioration of the degree of selective comminution for rod milling.

As shown in Fig. 9, ground samples produced by ball milling had smoother particle surfaces compared to those produce by rod milling, which exhibited relatively rough particle surfaces. In addition, the surface roughness factors (Λ) of 74–125 µm ground particles produced by ball and rod milling were 18.16 and 15.98, respectively. Rahimi et al. (2012) reported a similar result—the Λ value of ground particles from rod milling is greater than that of ball milling. Compared to ball milling, the increased grinding energy produced during rod milling increased the frequency of the fracturing of the feed material, promoting the formation of rough surfaces (Ahmed, 2010; Feng and Aldrich, 2000). By comparison, the presence of large numbers of fine particles increased the frequency of abrasion for ball milling, which was conducive to the generation of smoother and cleaner ground particle surfaces (Bu et al., 2019a, 2020a).

Fig. 10 displays a comparison of the shape characterizations of 74–125 μm ground particles produced

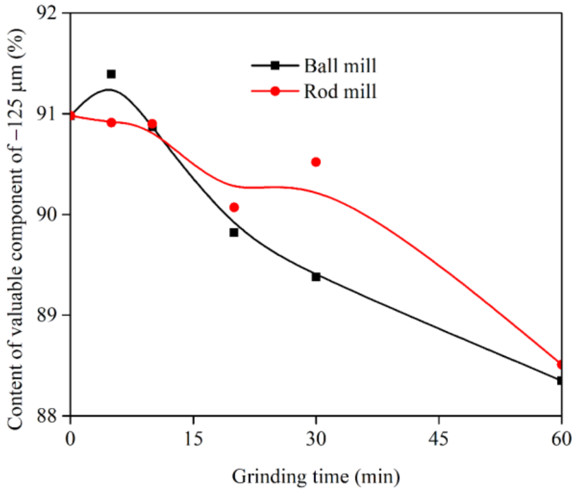

Fig. 8. Valuable component content of –125 μm ground particles produced by ball and rod milling

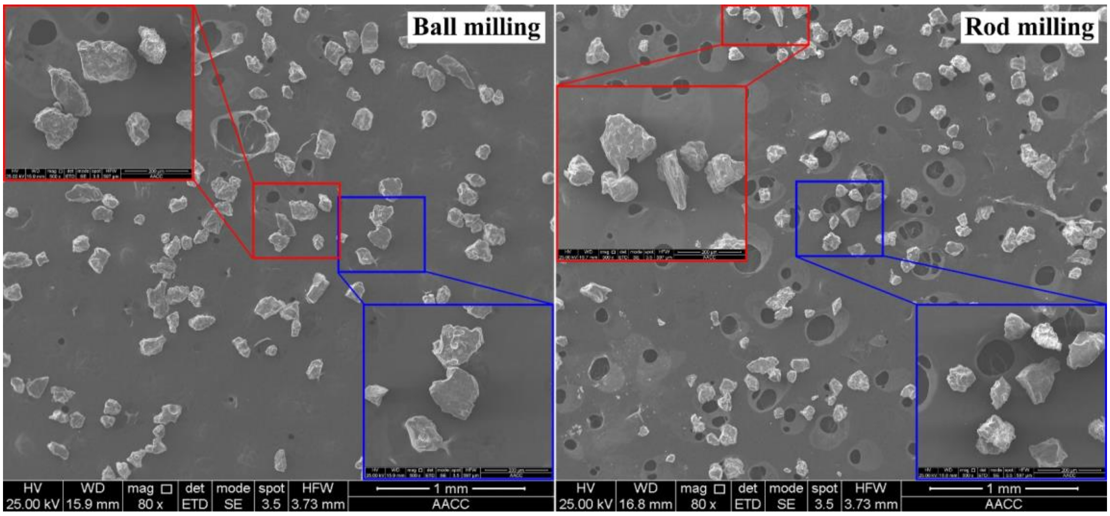

Fig. 9. SEM images of 74–125 μm ground particles produced by ball and rod milling at a grinding time of 10 min

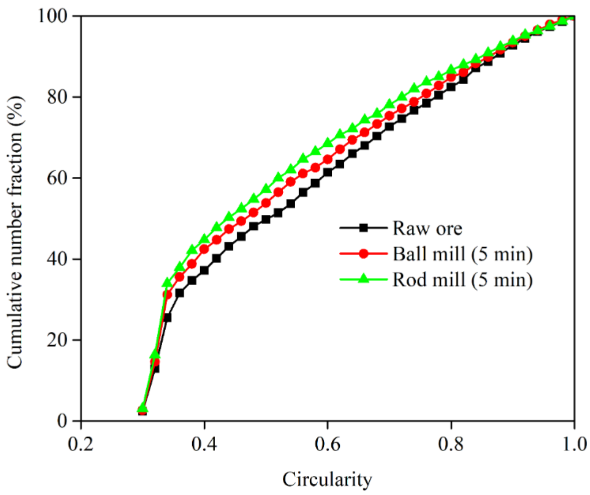

Fig. 10. Comparison of the circularity of the 74–125 μm ground product produced by ball and rod milling at a grinding time of 5 min

by ball and rod milling. The ground particles produced by rod milling were less circular than those produced by ball milling. Similar results have also been reported in the literature (Hicyilmaz et al., 2004; Ulusoy, 2008b; Ulusoy and Kursun, 2011). Further, particles of raw ore were rounder than the ground particles produced by ball rod milling. The ground particles produced by rod milling had a higher elongation ratio than those produced by ball milling, which was attributable to the different load models of ball and rod milling. Another reason for the higher elongation ratio for ground particles might be the increased breakage of round particles of the raw ore compared to those produced by ball milling.

4. Conclusions

In this work, the selective comminution of spent carbon anode (SCA) from aluminum electrolysis using ball and rod milling was investigated, in which comprehensive mineralogical, morphological, and chemical characterizations were conducted on the SCA sample to analyse the liberation of carbon from cryolite, and Fuerstenau upgrading curves assessment methods were used to compare the different degrees of selective comminution between ball and rod milling. The study revealed the following:

(1) Carbon particles (d_{50} = 46.86 μm) are embedded in mineral particles (major mineral: cryolite).

(2) An exponential asymmetric Eq. is capable of comparing the Fuerstenau upgrading curves quantitatively under different conditions. The comparative results indicate that ball milling is superior to rod milling in terms of selective comminution. When grinding is performed with a high energy input, rod milling is more conductive to breaking stronger minerals (carbon) as compared to ball milling, which, in turn, is harmful to achieving selective comminution via the different breakage rates of the stronger mineral and the weaker.

(3) Rod milling with a high grinding energy is conducive to the fracturing of large particles into two intermediate-sized particles, resulting in the formation of elongated particles with rough surfaces. While ball milling produced ground particles of smooth surfaces due to the higher frequency of abrasion, as evidenced by the presence of a large number of fines in the milling products.

Acknowledgment

This work was supported by the Fundamental Research Funds for the Central Universities (2018QNA16)

Appendix

Table 1s Original data for the Fuerstenau upgrading curves for ball milling (applied to the coarse fraction)

Cut size (mm)	Grinding time											
	0 min		5 min		10 min		20 min		30 min		60 min	
	R_W	R_V	R_W	R_V	R_W	R_V	R_W	R_V	R_W	R_V	R_W	R_V
1	0	0	0	0	0	0	0	0	0	0	0	0
0.5	5.17	0.40	6.04	0.26	7.15	0.25	2.60	0.10	2.57	0.27	0.00	0.00
0.25	28.16	11.18	20.72	1.52	19.42	1.38	7.67	0.49	6.31	0.44	2.84	0.43
0.125	57.11	39.38	44.69	17.70	38.11	13.73	25.51	7.86	17.41	2.57	6.85	0.97
0.074	80.46	71.18	73.26	55.43	61.31	44.46	45.31	25.31	42.21	23.57	20.67	3.98
0.045	85.27	79.56	82.02	69.30	72.58	62.26	57.88	42.44	52.28	37.34	35.09	12.73
0	100.00	100.00	100.00	100.00	100.00	100.00	100.00	100.00	100.00	100.00	100.00	100.00

Table 2s. Original data for the Fuerstenau upgrading curves for rod milling (applied to the coarse fraction)

Cut size (mm)	Grinding time											
	0 min		5 min		10 min		20 min		30 min		60 min	
	R_W	R_V	R_W	R_V	R_W	R_V	R_W	R_V	R_W	R_V	R_W	R_V
1	0	0	0	0	0	0	0	0	0	0	0	0
0.5	5.17	0.40	8.66	0.93	12.23	0.92	0.00	0.00	0.00	0.00	0.00	0.00
0.25	28.16	11.18	35.61	15.11	30.80	13.74	10.68	1.34	4.88	0.39	0.00	0.00
0.125	57.11	39.38	60.88	45.20	63.94	49.53	41.90	26.18	41.06	21.18	7.70	0.41
0.074	80.46	71.18	79.70	70.88	78.23	67.41	62.59	53.88	60.09	46.66	28.09	9.86
0.045	85.27	79.56	89.25	84.14	87.25	82.39	71.50	66.89	68.04	61.37	46.56	36.72
0	100.00	100.00	100.00	100.00	100.00	100.00	100.00	100.00	100.00	100.00	100.00	100.00

References

ABOUZEID, A.-Z. M. & FUERSTENAU, D. W., 2012, *Flow of materials in rod mills as compared to ball mills in dry systems*. Int. J. Miner. Process. 102-103, 51-57

AHMED, M. M., 2010, *Effect of comminution on particle shape and surface roughness and their relation to flotation process*. Int. J. Miner. Process. 94, 180-191

BISHOYI, N. 2015. *Treatment of spent pot lining by chemical leaching using nitric acid for enrichment of its fuel value and optimzation of the process parameters*. Bachelor of Technology, Department of Chemical Engineering, National Institute of Technology, Rourkela, India.

BRUNO, M. J., *Aluminum carbothermic technology comparison to hall-heroult process*. Symposium, Light metals. Warrendale, Pa., 2003. pp 395-400

BU, X., XIE, G., PENG, Y. & CHEN, Y., 2016, *Kinetic modeling and optimization of flotation process in a cyclonic microbubble flotation column using composite central design methodology*. Int. J. Miner. Process. 157, 175-183

BU, X., EVANS, G., XIE, G., PENG, Y., ZHANG, Z., NI, C. & GE, L., 2017, *Removal of fine quartz from coal-series kaolin by flotation*. Appl. Clay. Sci. 143, 437-444

BU, X., CHEN, Y., MA, G., SUN, Y., NI, C. & XIE, G., 2019a, *Differences in dry and wet grinding with a high solid concentration of coking coal using a laboratory conical ball mill: Breakage rate, morphological characterization, and induction time* 30, 2703-2711

BU, X., MA, G., PENG, Y., XIE, G., ZHAN, H. & LIU, B., 2019b, *Grinding kinetics of coal in wet ball-milling using the Taguchi method* Int. J. Coal Prep. Util.

BU, X., CHEN, Y., MA, G., SUN, Y., NI, C. & XIE, G., 2020a, *Wet and dry grinding of coal in a laboratory-scale ball mill: Particle-size distributions*. Powder Technol. 359, 305-313

BU, X., WANG, X., ZHOU, S., LI, B., ZHAN, H. & XIE, G., 2020b, *Discrimination of six flotation kinetic models used in the conventional flotation and carrier flotation of −74 μm coal fines*. ACS Omega 5, 13813-13821

CHAI, D., HOU, G. & HUANG, H., 2016, *Experimental study on the treatment of aluminum reduction carbon residue by vacuum metallurgy (in Chinese)*. Light Metals, 25-27

CHANG, J., LI, H., ZHENG, K., LIU, C., WANG, L., LI, B., BU, X. & SHAO, H., 2020, *Mineralogical characterisation and separation studies on the recovery of Cr2O3 in the high carbon ferrochrome slag*. Physicochem. Probl. Mineral Pro. 56, 460-470

CHEN, X., ZHAO, L. & LUO, Z., 2009, *Study on recycling process for electrolyte in carbon dust from reduction cells (in Chinese)*. Light Metals, 21-25

DRZYMALA, J. & AHMED, H. A. M., 2005, *Mathematical Eqs. for approximation of separation results using the Fuerstenau upgrading curves*. Int. J. Miner. Process. 76, 55-65

DUNBAR, C. A. & HICKEY, A. J., 2000, *Evaluation of probability density functions to approximate particle size distributions of representative pharmaceutical aerosols*. J. Aerosol. Sci. 31, 813-831

FENG, D. & ALDRICH, C., 2000, *A comparison of the flotation of ore from the Merensky Reef after wet and dry grinding*. Int. J. Miner. Process. 60, 115-129

FLORES, I. V., FRAIZ, F., JUNIOR, R. A. L. & BAGATINI, M. C., 2017, *Evaluation of spent pot lining (SPL) as an alternative carbonaceous material in ironmaking processes*. J. Mater. Res. Technol. 8, 33-40

FOSZCZ, D. & GAWENDA, T., 2012, *Analysis of efficiency of grinding in ball and rod mills dependably on contents of fine particles in feed*. AGH J. Min. & Geoengin. 36, 17-30

FOSZCZ, D., KRAWCZYKOWSKI, D., GAWENDA, T., KASIŃSKA-PILUT, E. & PAWLOS, W., *Analysis of process of grinding efficiency in ball and rod mills with various feed parameters*. IOP Conference Series: Materials Science and Engineering. Zawiercie, Poland, 26-29, September 01, 2018, 2018. p 012031

GRJOTHEIM, K., KROHN, C., MALINOVSKY, M., MATIAISOVSKY, K. & THONSTAD, J. (1982) Aluminium electrolysis: fundamentals of the Hall-Héroult process. Aluminium-Verlag

GUNGOREN, C., OZDEMIR, O., WANG, X., OZKAN, S. G. & MILLER, J. D., 2019, *Effect of ultrasound on bubble-particle interaction in quartz-amine flotation system* 52, 446-454

GUPTA, A. & YAN, D. (2016) Mineral Processing Design and Operations (Second Edition): Chapter 8 - Tubular Rod Mills. Elsevier

GUPTA, V. K. & PATEL, J. P., 2015, *A one-parameter model for describing the residence time distribution of closed continuous flow systems characterized by nonlinear reaction kinetics: Rod and ball mills*. Powder Technol. 274, 163-172

GUVEN, O., OZDEMIR, O., KARAAGACLIOGLU, I. E. & ÇELIK, M. S., 2015, *Surface morphologies and floatability of sand-blasted quartz particles* 70, 1-7

HESSE, M. (2014) Selective comminution for pre-concentration at mineral processing. In International Forum-Competition of Young Researchers, working group "Mining equipment and mechanical engineering". St. Petersburg, Russia, National Mineral Resources University

HESSE, M., POPOV, O. & LIEBERWIRTH, H., 2017, *Increasing efficiency by selective comminution*. Miner. Eng. 103, 112-126

HICYILMAZ, C., ULUSOY, U. & YEKELER, M., 2004, *Effects of the shape properties of talc and quartz particles on the wettability based separation processes*. Appl. Surf. Sci. 233, 204-212

HICYILMAZ, C., ULUSOY, U., BILGEN, S. & YEKELER, M., 2005, *Flotation responses to the morphological properties of particles measured with three-dimensional approach*. Int. J. Miner. Process. 75, 229-236

HICYILMAZ, C., ULUSOY, U., BILGEN, S., YEKELER, M. & AKDOGAN, G., 2006, *Response of rough and acute surfaces of pyrite with 3-D approach to the flotation* 42, 393-402

HOLYWELL, G. & BREAULT, R., 2013, *An overview of useful methods to treat, recover, or recycle spent potlining*. JOM 65, 1441-1451

INSTITUTE, I. A. (2020) Primary aluminium production. http://www.world-aluminium.org/statistics/#data. Accessed 20 Aug 2020

JUAREZ, G., CHEN, P. & LUEPTOW, R., 2011, *Transition to centrifuging granular flow in rotating tumblers: A modified Froude number*. New J. Phys. 13, 053055

KALLON, D. V. V., GOVENDER, I. & MAINZA, A. N., 2011, *Circulation rate modelling of mill charge using position emission particle tracking*. Miner. Eng. 24, 282-289

LEIßNER, T., MüTZE, T. & PEUKER, U. A., 2014, *Nutzung der direkten Messung des Aufschlussgrades in Sortierkennfeldern*. Chemie Ingenieur Technik 86, 899-905

LI, N., LI, R., XIE, G., HOU, Y., YU, X., CHEN, L. & WANG, Z., 2013, *Separating carbon and electrolyte in spent pot linings by floatation*. Light Metals, 23-27

LI, Q., CUI, X. & GAO, W., 2015, *Countermeasures and origins of carbon residue in aluminum reduction production (in Chinese)*. Light Metals 11, 36-38

LOWES, C., ZHOU, J. & GALVIN, K. (2018) Gravity separation of gold ore using the REFLUX™ classifier to achieve coarse particle gangue rejection. In Chemeca 2018. Queenstown, New Zealand. pp 1-8

LU, H. & QIU, Z., 1997, *Study on comprehensive utilization technique for treating spent potlining of aluminium electrolysis cells by flotation method (in Chinese)*, 32-34

MALYSHEV, V. P., MAKASHEVA, A. M. & ZUBRINA YU, S., 2017, *Comparative analysis of the work of ball and rod mills on the basis of the probabilistic model of grinding of materials*. Complex Use Miner. Resour., 5-11

MEI, X., LI, J. & YU, Z., 2016, *The research on cycling carbon residue by floatation process (in Chinese)*. Light Metals, 28-30

PAULY, H., 1985, *Hardness of cryolite, chiolite, cryolithionite and other fluorides from Ivigtut, South Greenland*. B. Geol. Soc. Denmark 34, 145-150

PERSONNET, P. B., 2013, *Treatment and reuse of spent pot lining, an industrial application in a cement kiln*. John Wiley & Sons, Inc. pp 1049-1056

RAHIMI, M., DEHGHANI, F., REZAI, B. & ASLANI, M. R., 2012, *Influence of the roughness and shape of quartz particles on their flotation kinetics* 19, 284-289

REICHERT, M., GEROLD, C., FREDRIKSSON, A., ADOLFSSON, G. & LIEBERWIRTH, H., 2015, *Research of iron ore grinding in a vertical-roller-mill*. Miner. Eng. 73, 109-115

SHI, Z., WEI, L. I., XIANWEI, H. U., REN, B., GAO, B. & WANG, Z., 2012, *Recovery of carbon and cryolite from spent pot lining of aluminium reduction cells by chemical leaching*. Trans. Nonferr. Metal. Soc. China 22, 222-227

SINGH, P. K. & MAITRA, P. K., 1986, *Recovery of carbon, fluoride as well as pollution abatement by recycling the flotation tailings in aluminium smelters*. UNEP Ind. & Envron. 9, 20-22

SLEAP, S. B., TURNER, B. D. & SLOAN, S. W., 2015, *Kinetics of fluoride removal from spent pot liner leachate (SPLL) contaminated groundwater*. J. Environ. Chem. Eng. 3, 2580-2587

STEPANOV, A. L., SHINKORENKO, S. F., FROLOV, A. V. & KOCHETKOV, P. A., 1991, *Selective comminution of two-component mineral mixtures*. J. Min. Sci. 27, 202-207

TROPENAUER, B., KLINAR, D., SAMEC, N., GOLOB, J. & KORTNIK, J., 2019, *Sustainable waste-treatment procedure for the spent potlining (SPL) from aluminium production*. Mater. Tehnol. 53, 277-284

ULUSOY, U., YEKELER, M. & HIçYıLMAZ, C., 2003, *Determination of the shape, morphological and wettability properties of quartz and their correlations*. Miner. Eng. 16, 951-964

ULUSOY, U., 2008a, *Physical Attributes of Particles and Their Roles on Wetting and Flotation*. In Fine Particle Technology and Characterization. Ed M. Yekeler. Research Signpost. pp 213-230

ULUSOY, U., 2008b, *Application of ANOVA to image analysis results of talc particles produced by different milling*. Powder Technol. 188, 133-138

ULUSOY, U. & KURSUN, I., 2011, *Comparison of different 2D image analysis measurement techniques for the shape of talc particles produced by different media milling*. Miner. Eng. 24, 91-97

ULUSOY, U. & IGATHINATHANE, C., 2014, *Dynamic image based shape analysis of hard and lignite coal particles ground by laboratory ball and gyro mills*. Fuel Process. Technol. 126, 350-358

WALTON, O. R. & BRAUN, R. L., *Simulation of rotary-drum and repose tests for frictional spheres and rigid sphere clusters*. Proc. Joint DOE/NFS Workshop on Flow of Particulates and Fluids. Lawrence Livermore National Lab., CA, United States, 1993 pp 1-18

WIDIJATMOKO, S. D., GU, F., WANG, Z. & HALL, P., 2020, *Selective liberation in dry milled spent lithium-ion batteries*. Sustain. Mater. Technol. 23, e00134

XIAO, J., YUAN, J., TIAN, Z., YANG, K., YAO, Z., YU, B. & ZHANG, L., 2018, *Comparison of ultrasound-assisted and traditional caustic leaching of spent cathode carbon (SCC) from aluminum electrolysis*. Ultrason. Sonochem. 40, 21-29

XIE, M., LI, R., ZHAO, H., LIU, W., LU, T. & LIU, F., 2020, *Detoxification of spent cathode carbon blocks from aluminum smelters by joint controlling temperature-vacuum process*. J. Clean. Prod. 249, 119370

XU, H., FAN, L., ZHANG, Y., LIANG, H. & YI, S., 2009, *Analysis of sources of carbon residue and its control methods (in Chinese)*. Carbon. Tech. 28, 41-44

YANG, K., GONG, P., TIAN, Z., LAI, Y. & LI, J., 2020a, *Recycling spent carbon cathode by a roasting method and its application in Li-ion batteries anodes*. J. Clean. Prod. 261, 121090

YANG, K., GONG, P., XIN, X., TIAN, Z. & LAI, Y., 2020b, *Purifying spent carbon anode (SCA) from aluminum reduction industry by alkali fusion method to apply for Li-ion batteries anodes: From waste to resource*. J. Taiwan Inst. Chem. Eng. 116, 121-127

YANG, X., BU, X., XIE, G. & CHEHREH CHELGANI, S., 2021, *A comparative study on the influence of mono, di, and trivalent cations on the chalcopyrite and pyrite flotation*. J. Mater. Res. Technol-JMRT 11, 1112-1122

YEKELER, M. & ULUSOY, U., 2004, *Characterisation of surface roughness and wettability of salt-type minerals: calcite and barite* 113, 145-152

YUAN, J., XIAO, J., LI, F., WANG, B., YAO, Z., YU, B. & ZHANG, L., 2018, *Co-treatment of spent cathode carbon in caustic and acid leaching process under ultrasonic assisted for preparation of SiC*. Ultrason. Sonochem. 41, 608-618

ZHOU, J. 2015. *Study on aluminum carbon residue by bubbling fluidized bed technology*. Dissertation for the master degree, Chongqing University, Chongqing

ZOU, W., YANG, D.-J., LIU, J.-C., FU, W.-Q. & MU, X.-B., 2018, *Research progress of recycling of spent cathode from aluminum electrolysis cells (in Chinese)*. China Nonferr. Metall. 47, 62-64